NONLINEAR (TIME DOMAIN) AND LINEARIZED (TIME & FREQUENCY DOMAIN) SOLUTIONS TO THE COMPRESSIBLE EULER EQUATIONS IN CONSERVATION LAW FORM

Final Report
for
NASA Lewis Research Center

Grant No. NAG-3-767
Entitled
Three-Dimensional Unsteady Euler Solutions for Interacting Blade Rows

by

Kidambi Sreenivas
and
David L. Whitfield

Computational Fluid Dynamics Laboratory
Engineering Research Center for Computational Field Simulation
Mississippi State University,
Mississippi State, MS 39762

August 21, 1995

ABSTRACT

Two linearized solvers (time and frequency domain) based on a high resolution numerical scheme are presented. The basic approach is to linearize the flux vector by expressing it as a sum of a mean and a perturbation. This allows the governing equations to be maintained in conservation law form. A key difference between the time and frequency domain computations is that the frequency domain computations require only one grid block irrespective of the interblade phase angle for which the flow is being computed. This is achieved through the use of phase shifted periodic boundary conditions. As a result of this and due to the fact that the governing equations for this case are steady, frequency domain computations are substantially faster than the corresponding time domain computations. The linearized equations are used to compute flows in turbomachinery blade rows (cascades) arising due to blade vibrations. Numerical solutions are compared to linear theory (where available) and to numerical solutions of the nonlinear Euler equations.

CHAPTER I

INTRODUCTION

Blade vibration (the aeroelastic problem) and noise generation (the aeroacoustic problem) are both undesirable consequences of the unsteady flow processes that occur within a turbomachine and are, therefore, important concerns to the designer. The aeroelastic problem has received far more attention than the aeroacoustic problem because the former can lead to structural failure of the blading and possibly result in extensive damage to the engine [1]. An unsteady aerodynamic analysis intended for turbomachinery aeroelastic and aeroacoustic applications must be applicable over a wide range of structural geometries, mean–operating conditions, and unsteady excitation modes and frequencies. Because of the large number of parameters involved, the analysis must provide the necessary unsteady information both efficiently and economically.

To date, three different types of methods have been used to model the unsteady flows through cascades [2]. They are : 1) analytical, 2) semi–analytical, and 3) numerical. The degree of accuracy of each of these methods depends on how well the mathematical models which represent these methods describe the unsteady flowfield for flow through a vibrating cascade.

The first approach involves solving the partial differential equations which govern the flow in a cascade using methods of applied mathematics. Closed form solutions can be obtained for a handful of extremely simplified geometries and flow conditions and hence are of limited use for configurations of practical interest.

The second approach uses a combination of singularities distributed along the airfoil surfaces and wakes to model the steady and unsteady flow through a cascade. This reduces the governing equations to a set of integral equations involving kernel functions. Because of the complexity in determining these kernel functions, the mean flow through the cascade is assumed to be uniform or nearly uniform. Hence, the flow model often bears little resemblance to flows found in actual turbomachines.

The third approach is to discretize the field equations which describe the unsteady flow and solve them numerically. The advantage of this approach is that features such as blade loading, arbitrary airfoil shapes, and moving shocks are accounted for. This ability to analyze fairly general geometries comes only with considerable computational overhead. The computational methods can be further subdivided into 1) methods based on nonlinear governing equations and 2) methods based on a set of linearized equations. The methods based on the nonlinear governing equations are almost always time–marching, while those based on the linearized equations are time–marching (time-domain) or harmonic (frequency-domain). The nonlinear governing equations are used if the unsteadiness in the flow cannot be treated as a small–perturbation of the nominal mean flow (steady or periodic) through the cascade. If the small–perturbation assumption is valid, the nonlinear equations can be linearized about the mean flow, resulting in a set of linearized equations for the unsteady perturbations. For most cases of practical interest, the linearized equations are good enough. The harmonic method introduces the additional simplifying assumption that the unsteady flow perturbations are harmonic in time. This reduces the linearized governing equations to a set of time–independent partial differential equations (PDEs) for the complex amplitudes of the unsteady flow properties. The time–marching method, on the other hand, makes no such assumptions and solves for the unsteady

perturbations by marching the solution in time. Both these approaches have been used in the course of the present study.

This report is divided into seven chapters. Chapter 2 deals with the development of the governing equations for the time and frequency domain computations. Development of a high-resolution flux formulation and numerical computation of flux Jacobians is presented in Chapter 3. Chapter 4 covers the solution procedure used while Chapter 5 deals with boundary conditions (BC's) for the time and frequency domain computations. Representative results are shown in Chapter 6. In Chapter 7, some conclusions are drawn regarding the utility of the methods used in this research.

CHAPTER II

GOVERNING EQUATIONS

In this chapter, the governing equations for linearized problems (time and frequency domain) are developed. The Navier–Stokes equations can most accurately describe the complicated nature of steady and unsteady flows through turbomachinery. However, if the Reynolds number is sufficiently high and Prandtl number is of order unity, the Euler equations provide a good approximation to the behavior of the flow. The nonlinear Euler equations for a dynamic curvilinear grid are obtained by transforming the Euler equations from Cartesian coordinates to dynamic curvilinear coordinates [3],[4]. These equations form the basis for both the nonlinear (un)steady flows as well as for the linearization. Section 2.1 develops the linearized Euler equations (time domain) based on the small perturbation approach, the perturbation being about a nonlinear mean flow (obtained from a steady state/ unsteady (periodic) solution to the unsteady, nonlinear Euler equations). Section 2.2 develops the linearized Euler equations for frequency domain computations.

2.1 Linearized Euler Equations (time domain)

For illustration purposes, consider the one–dimensional Euler equations in Cartesian coordinates, that is,

$$\frac{\partial q}{\partial t} + \frac{\partial f}{\partial x} = 0 \tag{2.1}$$

where q is the Cartesian dependent variable vector and f is the Cartesian flux vector. To start the linearization process, the dependent variables are expressed as the sum of two components, namely, a meanflow component which, by definition, satisfies the (un)steady nonlinear equations, and an unsteady perturbation, i.e.,

$$q = \overline{q} + q'$$

where the perturbations q' are assumed small compared to their mean–flow counterparts $\overline{q}$. Similarly, the flux can be viewed as being composed of two components, i.e.,

$$f = \overline{f} + f'$$

where $\overline{f}$ and f' are as yet undefined, but can be interpreted as mean and perturbed fluxes, respectively. A definition of f' based on a high resolution flux formulation will be given in Chapter III.

Using these definitions of q and f, and noting that the mean flow satisfies the equation,

$$\frac{\partial \overline{q}}{\partial t} + \frac{\partial \overline{f}}{\partial x} = 0$$

Equation (2.1) may be written as

$$\frac{\partial q'}{\partial t} + \frac{\partial f'}{\partial x} = 0 \tag{2.2}$$

Extending this approach to curvilinear coordinates results in

$$\frac{\partial Q'}{\partial \tau} + \frac{\partial F'}{\partial \xi} = 0 \tag{2.3}$$

$$\xi = \xi(x,\tau) \; ; \quad Q = J\, q \; ; \quad Q = \overline{Q} + Q'$$

$$F = J\,(\xi_x f + \xi_\tau q) \; ; \quad F = \overline{F} + F'$$

This extension is necessary because it is easier to handle arbitrary configurations in curvilinear coordinates as opposed to Cartesian coordinates. However, F is no longer a pure function of Q; it also depends on the metrics, i.e., ξ_τ and ξ_x. Hence, any definition of F' should take into account this dependency of F on the metrics. Extending Equation (2.3) to three–dimensions results in

$$\frac{\partial Q'}{\partial \tau} + \frac{\partial F'}{\partial \xi} + \frac{\partial G'}{\partial \eta} + \frac{\partial H'}{\partial \zeta} = 0 \tag{2.4}$$

Equation (2.4) is the linearized Euler equations (time domain) for three–dimensional curvilinear coordinates.

2.2 Linearized Euler Equations (frequency domain)

Expressing Q' and F' in Equation (2.3) as

$$Q' = \mathrm{Re}\left\{Q_0(\xi)\exp(i\omega\tau)\right\}$$

$$F' = \mathrm{Re}\left\{F_0(\xi)\exp(i\omega\tau)\right\}$$

results in

$$(i\omega)Q_0 + \frac{\partial F_0}{\partial \xi} = 0 \tag{2.5}$$

$i = \sqrt{-1}$

ω = frequency of vibration

Q_0, F_0 = Complex amplitudes of Q' and F' respectively

Equation (2.5) represents a steady-state equation for the complex amplitude Q_0. This equation is solved using a time marching method by introducing a pseudo-time derivative , i.e., we solve

$$\frac{\partial Q_0}{\partial \tau} + (i\omega)Q_0 + \frac{\partial F_0}{\partial \xi} = 0 \tag{2.6}$$

Equation (2.6) can be extended to three-dimensions resulting in

$$\frac{\partial Q_0}{\partial \tau} + (i\omega)Q_0 + \frac{\partial F_0}{\partial \xi} + \frac{\partial G_0}{\partial \xi} + \frac{\partial H_0}{\partial \xi} = 0 \tag{2.7}$$

Equation (2.7) is the linearized Euler equations (frequency domain) for three–dimensional curvilinear coordinates.

CHAPTER III

NUMERICAL FORMULATION

The governing equations for both the nonlinear and linearized cases can be written in the form

$$\frac{\partial \mathcal{Q}}{\partial t} + \frac{\partial \mathcal{F}}{\partial \xi} + \frac{\partial \mathcal{G}}{\partial \eta} + \frac{\partial \mathcal{H}}{\partial \zeta} = \mathcal{S} \tag{3.1}$$

where $\mathcal{Q} = Q$, $\mathcal{F} = F$, $\mathcal{G} = G$, $\mathcal{H} = H$ and $\mathcal{S} = 0$ correspond to the nonlinear case, $\mathcal{Q} = Q'$, $\mathcal{F} = F'$, $\mathcal{G} = G'$, $\mathcal{H} = H'$ and $\mathcal{S} = 0$ correspond to the linearized (time domain) case and $\mathcal{Q} = Q_0$, $\mathcal{F} = F_0$, $\mathcal{G} = G_0$, $\mathcal{H} = H_0$ and $\mathcal{S} = -i\omega Q_0$ correspond to the linearized (frequency domain) case. These governing equations are hyperbolic in time and can be solved by a time–marching technique.

3.1 Discretization of the Governing Equations

A finite volume semi–discretization of Equation (3.1) may be written as

$$\frac{\partial \mathcal{Q}}{\partial t} + \frac{\delta_i \mathcal{F}}{\Delta \xi} + \frac{\delta_j \mathcal{G}}{\Delta \eta} + \frac{\delta_k \mathcal{H}}{\Delta \zeta} = \mathcal{S} \tag{3.2}$$

where

$$\delta_* (.) = (.)_{*+\frac{1}{2}} - (.)_{*-\frac{1}{2}}$$

and i, j, k denotes a finite volume (cell) center. The * ± 1/2 denotes a cell interface and the dependent variables are assumed to be constant within each computational cell. In the curvilinear transformation the terms $\Delta\xi$, $\Delta\eta$ and $\Delta\zeta$ can be set equal to one and Equation (3.2) can be written as

$$\frac{\partial \mathcal{Q}}{\partial t} = -\mathcal{R} \tag{3.3}$$

where

$$\mathcal{R} = (\delta_i \mathcal{F} + \delta_j \mathcal{G} + \delta_k \mathcal{H} - \mathcal{S})$$

3.2 Flux formulation

The governing equations are hyperbolic in time, hence any flux formulation process should respect the direction of information propagation as dictated by the eigenvalues (upwinding). The approach used in this research is due to Roe [5]. It is based on a one–dimensional analysis of the Riemann problem, the idea being to solve an approximate Riemann problem exactly at each interface. The rest of this section is devoted to the development of formulas (first and second order spatial accuracy) for the fluxes at the cell faces for both the nonlinear and linearized Euler equations (time & frequency domain).

3.1.1 Flux formulas for nonlinear Euler equations

Details of the development of flux formulas (first and higher order) for the Euler equations are available from a variety of sources [5][6][7][8][9]. In particular, the formulation used in this research can be found in [6].

3.1.2 Flux formulas for linearized Euler equations (time domain)

Since the nonlinear unsteady Euler equations were solved using a high–resolution scheme based on Roe's approximate Riemann solver, it is logical to use a similar formulation for the linearized equations. The details of the linearization are available in [10]. The final form of the linearized flux formulation is:

$$\delta F' = F'_R - F'_L = \overline{A}(\overline{q}_R, \overline{q}_L, \overline{M}_\xi)\,(Q'_R - Q'_L) \tag{3.4}$$

where an overbar indicates a mean-flow quantity and a prime indicates a perturbed quantity. The perturbed flux at any face can then be computed as

$$F'_{i+\frac{1}{2}} = F'_L + \sum\nolimits^{-} a_j\, \bar{\lambda}^{(j)}\, \bar{r}^{(j)} \tag{3.5}$$

where

a_j = strength of the j$^{\text{th}}$ wave $= \bar{l}^{(j)} \cdot dQ'$

$\bar{\lambda}^{(j)}$ = j$^{\text{th}}$ eigenvalue of $\overline{A}(\overline{q}_R, \overline{q}_L, \overline{M}_\xi)$

$\bar{l}^{(j)}, \bar{r}^{(j)}$ = j$^{\text{th}}$ left and right eigenvectors of $\overline{A}(\overline{q}_R, \overline{q}_L, \overline{M}_\xi)$, respectively

M_ξ = Vector of metrics $\equiv [\xi_x, \xi_y, \xi_z, \xi_t]^T$

$Q' = \overline{J} q' + J' \overline{q}$

$dQ' = Q'_R - Q'_L$

and Σ^- denotes summation over the negative wave speeds. As can be seen from Equation (3.5), F'_L needs to be computed in order to evaluate $F'_{i+\frac{1}{2}}$. This can be achieved through a linearization of the flux vector, i.e.,

$$F_L = \overline{F}_L + J'\, A(\overline{q}_L, \overline{M}_\xi)\, \overline{q}_L + \overline{J}\, A(\overline{q}_L, \overline{M}_\xi)\, q'_L + \overline{J}\, R(\overline{q}_L, \overline{M}_\xi) M'_\xi$$

where

$$A(\overline{q}_L, \overline{M}_\xi) = \frac{\partial F}{\partial Q}\Big|_{\overline{q}_L, \overline{M}_\xi} \qquad \text{and} \qquad R(\overline{Q}_L, \overline{M}_\xi) = \frac{\partial F}{\partial \overline{M}_\xi}\Big|_{\overline{Q}_L, \overline{M}_\xi}$$

Noting that the flux (F_L) can be written as a sum of a mean and a perturbation results in the following definition for F'_L.

$$F_L{}' = J' A(\overline{q}_L, \overline{M}_\xi)\, \overline{q}_L + \overline{J} A(\overline{q}_L, \overline{M}_\xi)\, q'_L + \overline{J} R(\overline{q}_L, \overline{M}_\xi) M'_\xi$$

$$= A(\overline{q}_L, \overline{M}_\xi)\, Q'_L + R(\overline{Q}_L, \overline{M}_\xi) M'_\xi \qquad (3.6)$$

Similar formulas can be written for computing G' and H', thus extending this formulation to multiple-dimensions. Higher order fluxes are computed in a manner similar to the nonlinear fluxes and limiters are used to suppress spurious oscillations.

3.1.2 Flux formulas for linearized Euler equations (frequency domain)

Substituting for the "primed" quantities in Equations (3.5) and (3.6), we have

$$F'_{i+\frac{1}{2}} = F_0 \exp(i\omega\tau) \quad \text{and} \quad F_0 = \left[(AQ_{L0} + RM_{\xi_0}) + \sum\nolimits^{-} a_j \bar{\lambda}^{(j)} \bar{r}^{(j)} \right] \qquad (3.7)$$

where

a_j = strength of the j$^{\text{th}}$ wave $= \bar{l}^{(j)} \cdot dQ_0$

$\bar{\lambda}^{(j)}$ = j$^{\text{th}}$ eigenvalue of $\overline{A}$

$\bar{l}^{(j)}, \bar{r}^{(j)}$ = j$^{\text{th}}$ left and right eigenvectors of $\overline{A}$, respectively

$dQ_0 = Q_{R0} - Q_{L0}$

Further,

$$M'_\xi = M_{\xi_0} \exp(i\omega\tau)$$

$$M_{\xi_0} = \left[\xi_{x0}, \xi_{y0}, \xi_{z0}, \xi_{t0} \right]^T$$

where ξ_{x0} etc. are complex numbers and represent the harmonic deformation of the grid due to the vibration of the body. Formulas similar to F' can be written for G' and H' also. Higher order accurate fluxes are computed using simple extrapolation. Limiters are not used because using them introduces nonlinearities which prevent certain simplification from being made.

CHAPTER IV

SOLUTION PROCEDURE

In this chapter, time discretization of Equation (3.2) is carried out. A broad class of difference schemes for advancing the solution in time is given by

$$\frac{(1+\psi)\Delta\mathcal{Q}^n - \psi\Delta\mathcal{Q}^{n-1}}{\Delta\tau} = (\theta-1)\mathcal{R}^n - \theta\mathcal{R}^{n+1} \tag{4.1}$$

Some of the implicit time differencing schemes represented are three–point backward ($\theta = 1, \psi = 1/2$), backward Euler ($\theta = 1, \psi = 0$), and trapezoidal ($\theta = 1/2, \psi = 0$). Accounting for deforming grids [10] results in

$$\Delta q^n = \frac{1}{1+\psi}\left\{ \frac{\Delta\tau}{J^{n+1}}\left[(\theta-1)\mathcal{R}^n - \theta\mathcal{R}^{n+1} \right] + \psi\left[\frac{J^{n-1}}{J^{n+1}}\,\Delta q^{n-1} + q^n\,\frac{\Delta J^{n-1}}{J^{n+1}}\right]\right\}$$

$$- q^n\frac{\Delta J^n}{J^{n+1}} \tag{4.2}$$

where q is the Cartesian dependent variable vector. Rewriting Equation (4.2) in operator form and applying Newton's method (for time accuracy) to the resulting equation, we have [10] (for the nonlinear Euler equations)

$$\left[\frac{1+\psi}{\theta}\,\frac{I}{\overline{\Delta\tau}} + \delta M^+\cdot + \delta M^-\cdot\right]\Delta q^{n+1,m} = -RHS(q^{n+1,m}) \tag{4.3}$$

where

$$RHS(q^{n+1,m}) = \frac{1+\psi}{\theta\,\overline{\Delta\tau}}\left(q^{n+1,m} - q^n\right) - \frac{1}{\theta}\left[(\theta-1)R^n - \theta R^{n+1,m}\right]$$

$$- \frac{\psi}{\theta\,\overline{\Delta\tau}}\,\frac{J^{n-1}}{J^{n+1}}\,\Delta q^{n-1} + \frac{1+\psi}{\theta\,\overline{\Delta\tau}}\,\frac{q^n}{J^{n+1}}\left[\Delta J^n - \frac{\psi}{1+\psi}\Delta J^{n-1}\right]$$

$$\overline{\Delta\tau} = \frac{\Delta\tau}{J^{n+1}}$$

and m represents the Newton iteration parameter. Adopting the same approach for the linearized Euler equations (time-domain) results in

$$\left[\frac{1+\psi}{\theta}\,\frac{\overline{J}}{\Delta\tau}I + \delta\overline{M}^+\cdot + \delta\overline{M}^-\cdot\right]\Delta q'^{n+1,m} = -RHS(q'^{n+1,m}) \tag{4.4}$$

where the overbar for the M's implies mean flow based quantities and

$$RHS(q'^{n+1,m}) = \frac{\overline{J}}{\Delta\tau}\left[q'^{n+1,m} - q'^n\right] - \frac{\overline{J}}{1+\psi}\left[(\theta-1)\tilde{R}'^n - \theta\tilde{R}'^{n+1,m}\right]$$

$$- \frac{\overline{J}}{\Delta\tau}\,\frac{\psi}{1+\psi}\Delta q'^{n-1}$$

The linearized (frequency domain) Euler equations are solved using local time stepping and Newton's method need not be used (since we desire only steady-state solutions). The discretized frequency domain equations can be written as

$$\left[\frac{1+\psi}{\theta}\,\frac{\overline{J}}{\Delta\tau}I + \delta\overline{M}^{+}\cdot + \delta\overline{M}^{-}\cdot\right]\Delta q_0^n = -R_0(q_0^n) \tag{4.5}$$

where R_0 is the complex residual. The $\delta M^{\pm}$ in all these equations can be defined as

$$\delta M^{+}\cdot = \delta_i A^{+}\cdot + \delta_j B^{+}\cdot + \delta_k C^{+}\cdot$$

$$\delta M^{-}\cdot = \delta_i A^{-}\cdot + \delta_j B^{-}\cdot + \delta_k C^{-}\cdot$$

4.1 Choice of Flux Jacobians

The flux Jacobians can be obtained from the flux vector split (FVS) form or the flux difference split (FDS) form. The final form of the Jacobians using these two formulations are:

FVS:

$$A^{\pm} = \frac{\partial F^{\pm}(q^{n+1,m})}{\partial q^{n+1,m}} \qquad B^{\pm} = \frac{\partial G^{\pm}(q^{n+1,m})}{\partial q^{n+1,m}} \qquad C^{\pm} = \frac{\partial H^{\pm}(q^{n+1,m})}{\partial q^{n+1,m}}$$

FDS:

$$A^{\pm} = \frac{\partial F_{i+\frac{1}{2}}}{\partial q_{i+p}}\Big)_m \qquad B^{\pm} = \frac{\partial G_{j+\frac{1}{2}}}{\partial q_{j+p}}\Big)_m \qquad C^{\pm} = \frac{\partial H_{k+\frac{1}{2}}}{\partial q_{k+p}}\Big)_m$$

where $p = 0$ for M^{+} and $p = 1$ for M^{-} and m is the Newton iteration parameter.

4.2 Solution of Linear Systems

Equations (4.3), (4.4) and (4.5) can be written in a general form as

$$(L + D + U)\,x = b \tag{4.6}$$

where L is strictly lower block triangular, D is block diagonal and U is strictly upper block triangular. This system defined by Equation (4.6) can be solved using the "N–Pass" algorithm. The "N–Pass" algorithm can be viewed as a relaxation scheme based on the symmetric Gauss–Seidel algorithm:

$$\left.\begin{aligned}(L + D)\,x^1 + U\,x^0 &= b\\ (D + U)\,x^2 + L\,x^1 &= b\end{aligned}\right\}\ \text{1st pass}$$

$$\vdots \tag{4.7}$$

$$\left.\begin{aligned}(L + D)\,x^{2N-1} + U\,x^{2N-2} &= b\\ (D + U)\,x^{2N} + L\,x^{2N-1} &= b\end{aligned}\right\}\ \text{Nth pass}$$

with $x^0 = 0$. The nature of L, D and U can be exploited to reduce the number of matrix–vector multiplications to be carried out [10].

CHAPTER V

BOUNDARY CONDITIONS

The problem of determining a solution to a partial differential equation when both initial and boundary data are present is called an *initial–boundary value problem* [11]. The solution to the Euler equations on finite domains falls under this category of problems. Boundary conditions are vital in determining the success or failure of a CFD code. Incorrect boundary conditions can often lead to wrong solutions or at least drastically alter convergence rates. Boundary conditions (BC's) can be classified into three major categories: 1) Far field BC's (inflow/outflow) 2) Solid wall BC's (no flow across a surface) 3) Block–to–block BC's (transfer boundary conditions).

The Euler equations are hyperbolic in time. This means that the characteristics determine the direction of propagation of information from or to the boundaries. Therefore, it is only natural to use a formulation based on characteristic variables to determine the physical and numerical boundary conditions to be imposed at any given boundary. The formulation and implementation of far field conditions for steady flows is identical to that used in [12] and will not be repeated here.

This chapter is divided into four sections. The first section deals with the development of non-reflecting far field boundary conditions for unsteady flows (time domain) as well as for the frequency domain. Sections 2 and 3 deal with development of impermeable wall BC's for nonlinear and linearized flows respectively. The last section explains the multi-block strategy for the unsteady (time domain) cases and how the computations can be performed in just one grid block for the frequency domain cases.

5.1 Non–Reflecting Boundary Conditions

The two–dimensional Euler equations (Cartesian coordinates) in nonconservative, quasilinear form can be written as

$$\frac{\partial U}{\partial t} + a\,\frac{\partial U}{\partial x} + b\,\frac{\partial U}{\partial y} = 0 \tag{5.1}$$

where $U = (\varrho, u, v, p)^T$ and

$$a = \begin{bmatrix} u & \varrho & 0 & 0 \\ 0 & u & 0 & \frac{1}{\varrho} \\ 0 & 0 & u & 0 \\ 0 & \gamma p & 0 & u \end{bmatrix} \qquad b = \begin{bmatrix} v & 0 & \varrho & 0 \\ 0 & v & 0 & 0 \\ 0 & 0 & v & \frac{1}{\varrho} \\ 0 & 0 & \gamma p & v \end{bmatrix}$$

Equation (5.1) can be linearized to yield (for small perturbations):

$$\frac{\partial U'}{\partial t} + a\,\frac{\partial U'}{\partial x} + b\,\frac{\partial U'}{\partial y} = 0 \tag{5.2}$$

where

$$U' = [\varrho', u', v', p']^T$$

and a and b are constant coefficient matrices based on the steady flow variables. Non–dimensionalization of Equation (5.2) results in:

$$a = \begin{bmatrix} u & 1 & 0 & 0 \\ 0 & u & 0 & 1 \\ 0 & 0 & u & 0 \\ 0 & 1 & 0 & u \end{bmatrix} \qquad b = \begin{bmatrix} v & 0 & 1 & 0 \\ 0 & v & 0 & 0 \\ 0 & 0 & v & 1 \\ 0 & 0 & 1 & v \end{bmatrix}$$

A Fourier analysis of Equation (5.2) (as described in [13]) yields a set of (four) eigenvectors representing an entropy wave, a vorticity wave, an upstream running pressure wave and a downstream

running pressure wave. Based on this analysis, the characteristic variables for unsteady flows can be written in terms of the perturbation variables as:

$$\begin{bmatrix} c_1 \\ c_2 \\ c_3 \\ c_4 \end{bmatrix} = \begin{bmatrix} -1 & 0 & 0 & 1 \\ 0 & 0 & 1 & 0 \\ 0 & 1 & 0 & 1 \\ 0 & -1 & 0 & 1 \end{bmatrix} \begin{bmatrix} \delta\varrho \\ \delta u \\ \delta v \\ \delta p \end{bmatrix} \tag{5.3}$$

where $\delta\varrho$, δu, δv and δp are the perturbations from the mean flow and the c_i 's are the characteristic variables. Using these eigenvectors and assuming locally one–dimensional flow at the boundary, the boundary condition, expressed in terms of the characteristic variables is simply

$$c_n = 0$$

for all n corresponding to incoming waves. This means that, for subsonic inflow, the amplitudes of incoming unsteady characteristics (c_1, c_2, c_3: assuming co-directional inflow) are set to zero and the outgoing characteristic is computed using Equation (5.3). For subsonic outflow, $c_4 = 0$ (again, assuming co-directional outflow) and the remaining characteristics are computed. Once the characteristics are known at the inflow as well as outflow boundaries, the perturbations can be determined using an inverse transform.

The primitive variables can now be calculated because the perturbations from the mean flow (i.e., $\delta\varrho$, δu, δv and δp) are known. Once the primitive variables have been determined, the conserved variables can be calculated. The strategy for the frequency domain case is very similar to that described here because the governing equations can be cast in terms of the nonconserved quantities, thereby yielding a set of equations identical to (5.2) except that the primed quantities are replaced by the corresponding complex quantities.

5.2 Solid Wall Conditions for Nonlinear Euler equations

Casting the non–conservative form of the nonlinear, Euler equations into characteristic variable form and assuming locally one–dimensional flow results in

$$\frac{\partial W_k}{\partial \tau} + \Lambda_k \frac{\partial W_k}{\partial k} = 0 \qquad k = \xi, \eta \text{ or } \zeta \tag{5.4}$$

where W_k are the characteristic variables. The details of the derivation and implementation are available from a variety of sources including [4], [12], [14] etc.

5.3 Solid Wall Conditions for Linearized Euler Equations

The linearized Euler equations can be written as

$$\frac{\partial Q'}{\partial \tau} + \sum_{k=\xi,\eta \text{ and } \zeta} K(\bar{q}_R, \bar{q}_L, M_k) \frac{\partial Q'}{\partial k} = 0 \tag{5.5}$$

where an overbar indicates a mean quantity and a prime a perturbation (a real number for time domain and a complex number for frequency domain) and $K = A$ for $k = \xi$, $K = B$ for $k = \eta$ and $K = C$ for $k = \zeta$, A, B and C being the flux Jacobians in the ξ, η and ζ directions respectively. Casting Equation (5.5) into characteristic variable form and assuming locally one–dimensional flow yields

$$\frac{\partial W_k'}{\partial \tau} + \Lambda_k \frac{\partial W_k'}{\partial k} = 0 \tag{5.6}$$

where

$$W_k' = T_{k,0}^{-1} Q' = [w'_{k,1}, w'_{k,2}, w'_{k,3}, w'_{k,4}, w'_{k,5}]^T$$

and

$$K = T_k \Lambda_k T_k^{-1}$$

The subscript 0 (zero) indicates a reference condition. An impermeable surface is characterized by zero normal velocity. Therefore, the first three eigenvalues are zero, the fourth positive and the fifth negative. Using this in Equation (5.6) yields

$$(w'_{k,1})_b = (w'_{k,1})_r \tag{5.7}$$

$$(w'_{k,2})_b = (w'_{k,2})_r \tag{5.8}$$

$$(w'_{k,3})_b = (w'_{k,3})_r \tag{5.9}$$

$$\left[k_x u + k_y v + k_z w + k_t\right]_b = 0 \tag{5.10}$$

$$(w'_{k,4})_b = (w'_{k,4})_r \tag{5.11}$$

or

$$(w'_{k,5})_b = (w'_{k,5})_r \tag{5.12}$$

where the subscripts b and r denote boundary and reference values respectively. In this case, the reference value is chosen as the center of the first cell off the boundary. If the point r is in the positive k direction from the boundary, Equation (5.12) is used, otherwise Equation (5.11) is used. Equations (5.7) through (5.9) are imposed conditions, i.e., they help in obtaining a set of five simultaneous equations that can be solved. Note that even though Equation (5.10) is written in terms of total quantities, a perturbed form of the same is used in the solution process. This is because the rest of the equations are in perturbed form. This system of equations (real or complex perturbations, but with real coefficients) is solved for the perturbations at the boundary.

5.4 Block–to–Block Boundary Conditions

Figure 5.1 represents a single grid block used for calculations with steady flows and flows with in–phase blade motions. All the cases considered in this study involved cascades. The boundaries that extend upstream and downstream of the airfoils are called *periodic boundaries*. Therefore, a periodic boundary condition is imposed between lines A–B and E–F, and C–D and G–H.

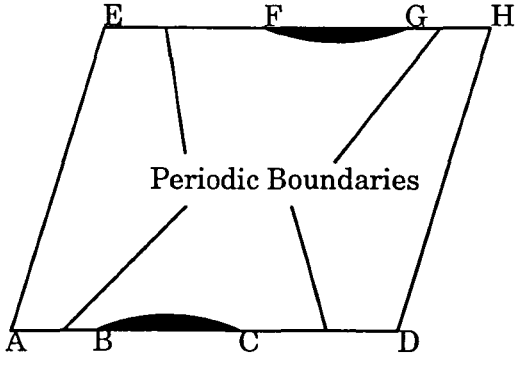

Figure 5.1 Periodic boundaries in a typical cascade

For harmonic blade motions with constant phase difference (interblade phase angle, σ) between adjacent blades, multiple blade rows (N of them) are required to simulate the flow field. The number of blade passages required for arbitrary σ is given by N = *smallest integer* { (360/σ), 360/(360 – σ) }.

For example, for $\sigma = 180°$, two grid blocks are required. For the frequency domain case, multiple grid blocks are unnecessary because a phase shifted boundary condition can be applied at the periodic boundaries thereby enabling computations to be performed in just one grid block.

CHAPTER VI

RESULTS

Various test cases were used to validate the applicability of the present method for solving problems involving aeroelastic and aeroacoustic phenomena. The test cases selected cover a wide range of geometries as well as flow conditions. This chapter is divided into three main sections. The first section deals with uniform mean flows, while the second one deals with nonuniform mean flows (flows with blade loading). The last section discusses the performance of the linearized solver with respect to the nonlinear solver. In both cases, the unsteadiness in the flow field is due to blade motion. The blades oscillate according to:

$$h_y = h_{0y} \sin(\omega t + \sigma) \qquad \text{for tangential (plunging) motion}$$

$$\alpha = \alpha_0 \sin(\omega t + \sigma) \qquad \text{for torsional (pitching) motion}$$

where h_{0y} and α_0 are the respective amplitudes, ω the circular frequency of oscillation and σ the inter-blade phase angle. These oscillations are captured using a locally deforming grid technique [10].

As a part of the code validation process, linearized results are compared with linear theory for a cascade of flat plates. Linearized Euler computations are also compared with nonlinear Euler solutions for a cascade of airfoils, for which no theoretical results are available. The computations typically required 4 cycles of motion with 200 time steps/cycle (for time domain) and 200 pseudo time steps (for frequency domain) to reach a periodic/steady state. A schematic of a typical two–dimensional cascade defining various terms used in this chapter is shown in Figure 7.1.

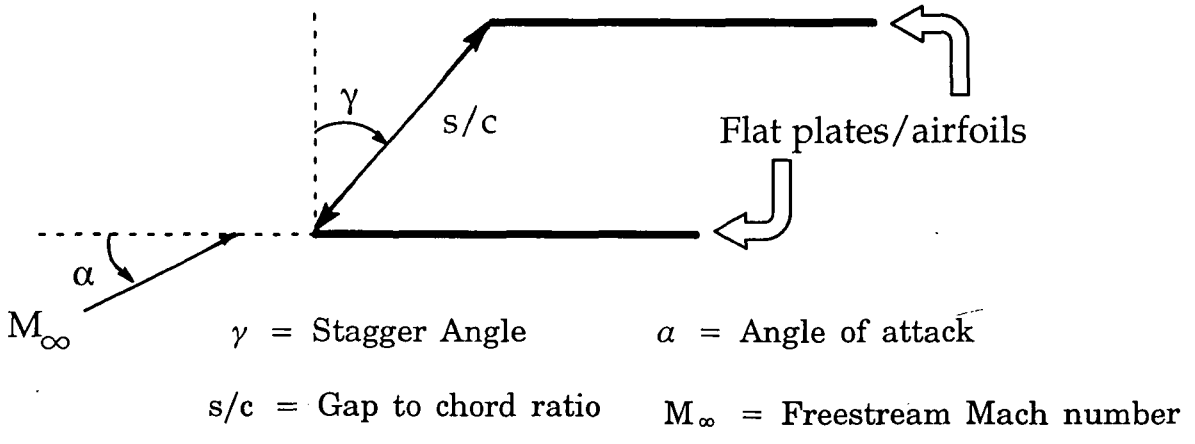

Figure 7.1 Schematic of a typical cascade

7.1 Uniform Mean Flows

For the set of cases considered in this section, the mean flow is uniform, i.e., the cascade under consideration is made up of infinitely thin flat plates and is at zero degree angle of attack. For these cases, theoretical results ([15],[16]) for supersonic as well as subsonic axial flows are available, hence, they form a basis for the validation of the present method. The computer program of [15] is based on the theory developed by Lane [17]. Unless otherwise mentioned, all computations were performed on a 71x51 H–grid, with 50 points on either face of the flat plate.

7.1.1 High solidity cascade, Plunging motion, M_∞=2.61

Linearized results (time domain) are first compared to available theoretical results for a high–solidity cascade with a supersonic axial flow. The cascade is oscillating in plunge, has a gap–to–chord ratio of 0.311 and a stagger of 28°. The freestream Mach number is 2.61, the interblade phase angle is 90°, and the reduced frequency (κ) based on semi–chord is 0.5. The maximum CFL used was 5. As can be seen from Figure 7.2, excellent agreement is seen between theory and the linearized solver (time domain). The location as well as the strength of the real and imaginary parts of the discontinuities are captured accurately by the linearized solver.

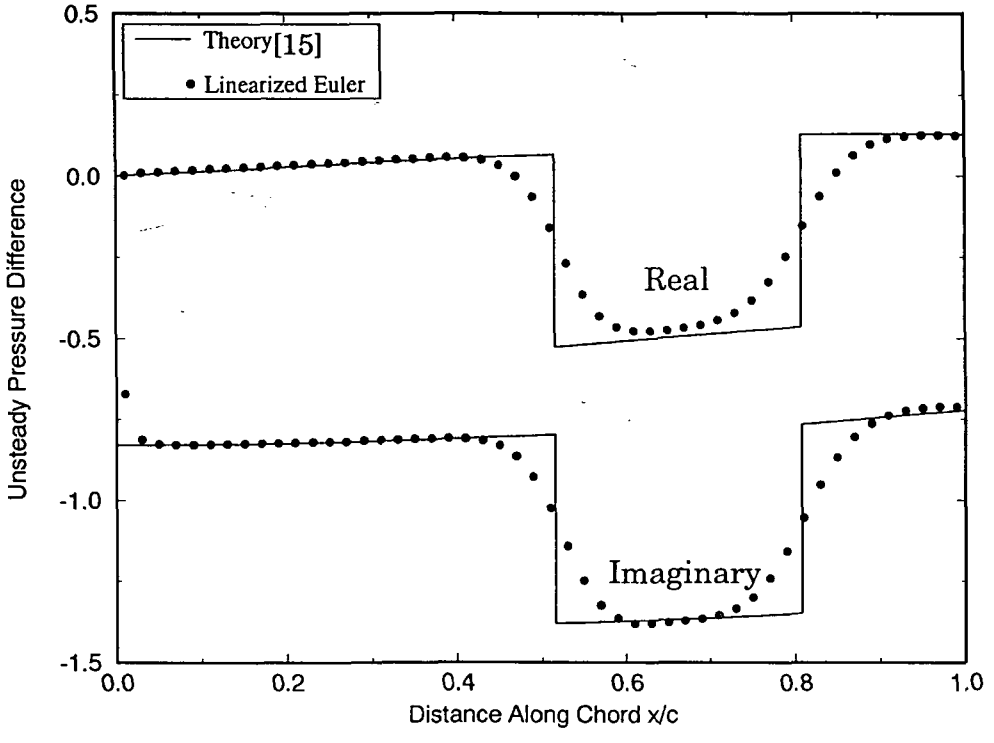

Figure 7.2 Unsteady pressure difference on a flat plate cascade due to plunging motion (M_∞=2.61, s/c=0.311, γ=28°, κ=0.5 and σ = 90°)

7.1.2 Low solidity cascade, Pitching motion, M_∞=0.8

This case involves a cascade oscillating in pitch at a reduced frequency of 1.5 with an interblade phase angle of 270°. The cascade geometry is identical to that used in the previous test case and the free stream Mach number is 0.8. A higher resolution grid (121x41) was used in this computation and the maximum CFL was 3.25. The comparison is shown in Figure 7.3. The computed results (time domain) are in good agreement with the theoretical predictions.

7.2 Nonuniform Mean Flows

Nonuniformity in a mean flow field can be caused either by the cascade being at an angle of attack or by the cascade being composed of airfoils (not infinitely thin flat plates) or a combination of the two. Since the mean flow is not uniform any more, it needs to be computed. This is done using the high

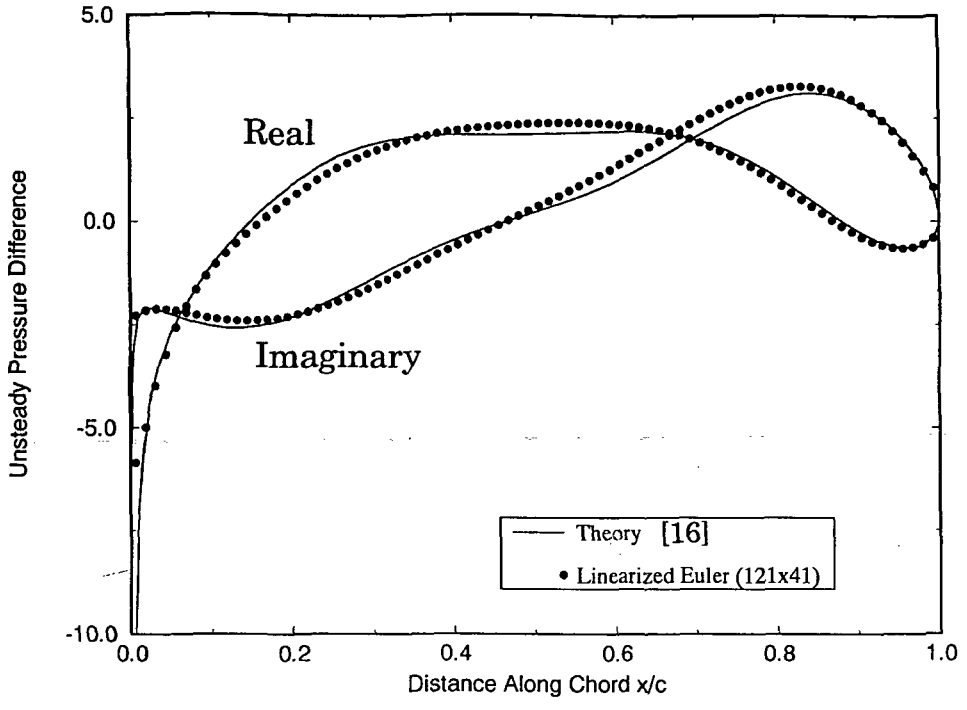

Figure 7.3 Unsteady pressure difference on a flat plate cascade due to pitching motion (M_∞=0.8, s/c=1.0, γ=45°, κ=1.5, σ = 270° and pitching axis @ 30% chord)

resolution, flux difference split, time–marching solver, which upon convergence yields the required steady state/unsteady (periodic) mean flow field. All steady flow computations were performed on a single block grid, while the unsteady calculations required multiple grid blocks depending on the inter-blade phase angle. The frequency domain computations were performed om a single block grid. This rest of this section deals with the so called 10th standard configuration.

The 10th standard configuration (10th std. cfg.) consists of a cascade of modified NACA 0006 airfoils. The gap–to–chord ratio is 1.0 and the stagger angle is 45°. All computations were performed using a 121x41 H–grid, with 60 points each on the pressure and suction surfaces. The maximum CFL used in the steady mean flow computations was 5000 (with local time stepping), while for the unsteady cases it was 85. The cascade geometry and the multi–block grid used in the computation is shown in Figure 7.4.

7.2.1 Tenth standard configuration: Subsonic case

The cascade is in a flow with M_∞=0.7 and at a 10° angle of attack. The mean flow through the cascade is subsonic and reaches a maximum Mach number of 0.92 on the suction surface. A back pressure (ratio of p_{exit} to p_{total}) of 0.87 was used to achieve the required Mach number (0.7 in this case) at the inlet. It was also observed that the back pressure required was a function of the configuration being considered as well as the grid used for the computation. The steady pressure distribution for this case is shown in Figure 7.5. For the unsteady calculations, the cascade is set into motion in plunge or pitch. The amplitudes of plunge and pitch are 1% chord and 1° respectively. These cases are considered next.

Plunging motion, κ = 0.6435, σ = –90°:

The cascade is oscillated in plunge at a semi–chord reduced frequency of 0.6435 and an inter-blade phase angle of –90°. The real and imaginary parts of the first harmonic of the unsteady pressure

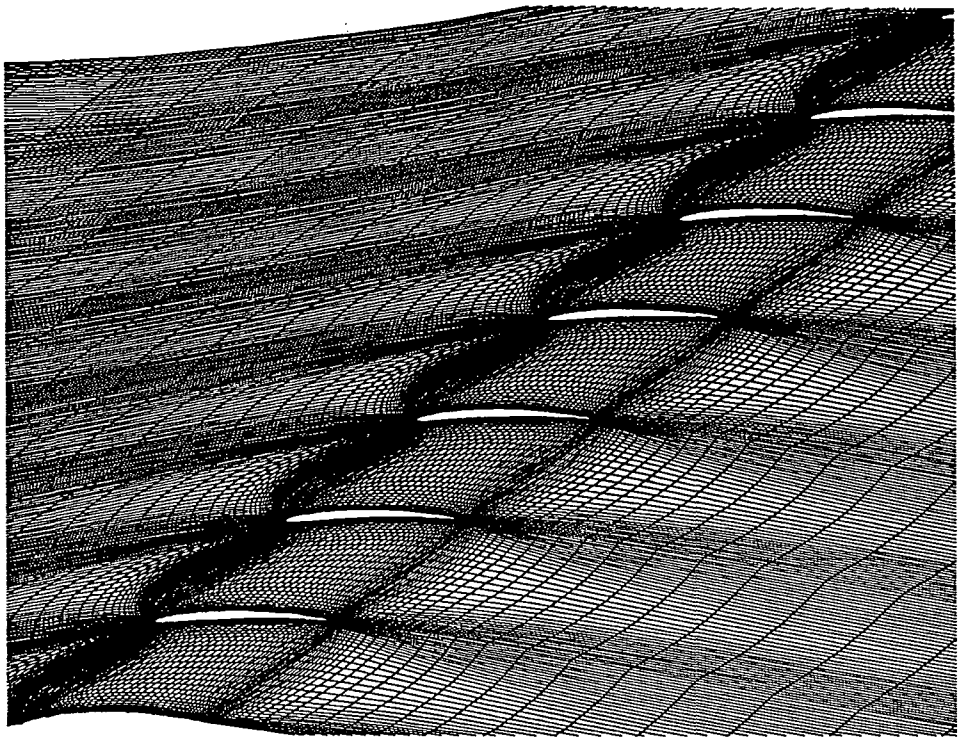

Figure 7.4 Cascade geometry and multi–block grid used in computation

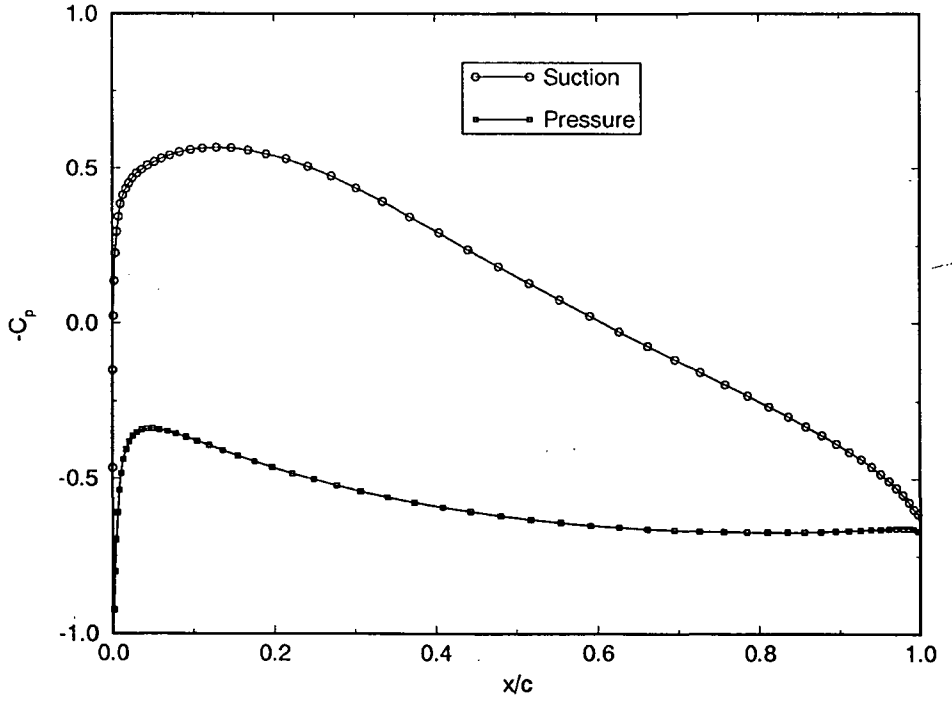

Figure 7.5 Steady pressure distribution for subsonic 10th standard configuration cascade

distribution are shown in Figure 7.6 and Figure 7.7 respectively. As can be seen from these two figures, the agreement between the linearized and nonlinear solution is very good.

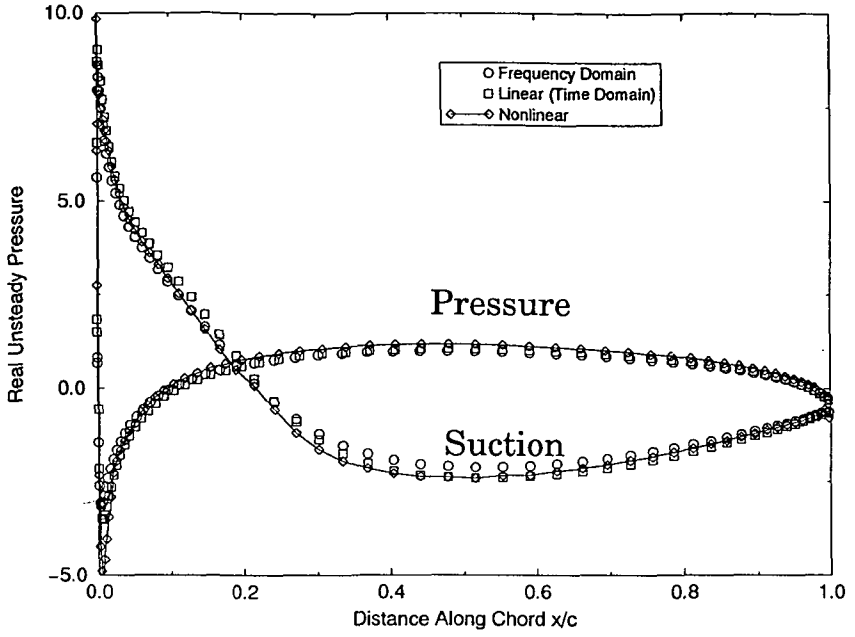

Figure 7.6 Real part of unsteady pressure distribution on subsonic 10th std. cfg. due to plunging motion (κ=0.6435, σ=–90°)

7.2.2 Tenth standard configuration: Transonic case

The second case is a transonic cascade (M_∞=0.8, α=13°). This case is characterized by a fairly strong in–passage shock. A back pressure of 0.87 was found to be sufficient to achieve the required Mach number of 0.8 at the inlet. The pressure distribution for the transonic case is shown in Figure 7.8. The unsteady cases are considered next.

Plunging motion, κ = 0.6435, σ = -90°:

The cascade is pitching at a reduced frequency of 0.6435 and an interblade phase angle of –90°. Figure 7.9 shows the real part of the unsteady pressure distribution, while Figure 7.10 shows the imaginary part of the same. As can be seen from these two figures, reasonably good agreement is achieved between the nonlinear and linearized Euler solutions. It was observed that for the cases considered, the linearized solutions were scalable with respect to the amplitudes of pitch or plunge as the case may be, but the nonlinear solutions exhibited a dependency on the amplitudes used (mainly near discontinuities).

6.4 Comparison of the Various Approaches Used

The linearized (time-domain) code required about 14 minutes of CPU time (for a 4 block, 121x41 grid) on a CRAY-YMP to reach a periodic state. For the same problem, the nonlinear code required about 20 minutes of CPU time. The linearized (frequency domain) code, on the other hand, required only about 1 minute of CPU time (Note that computation in the frequency domain case requires only 1 grid block).

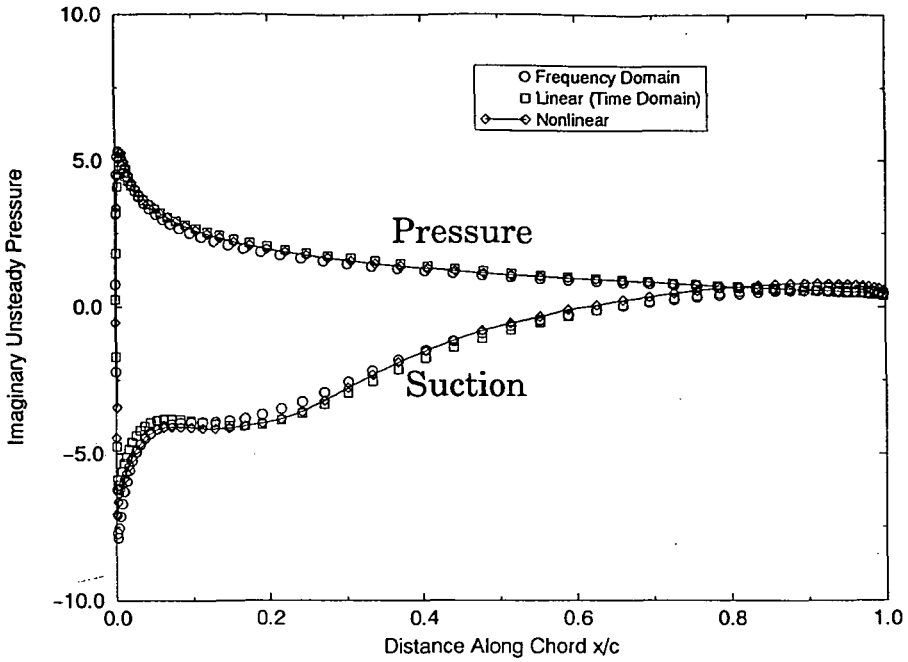

Figure 7.7 Imaginary part of unsteady pressure distribution on subsonic 10th std. cfg. due to plunging motion (κ=0.6435, σ=–90°)

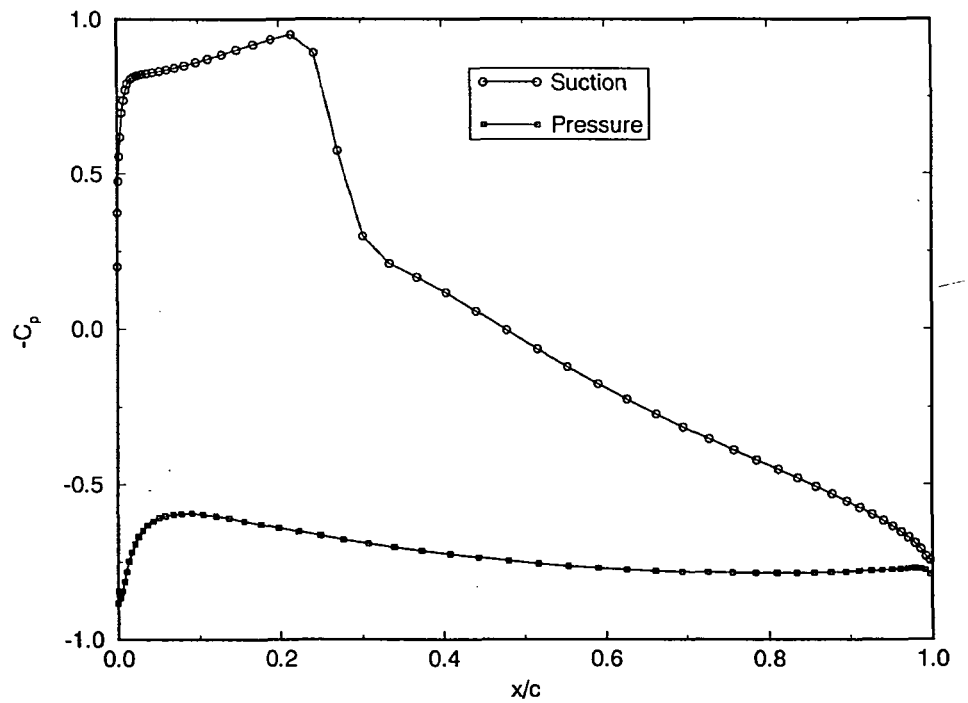

Figure 7.8 Steady pressure distribution for transonic 10th standard configuration cascade

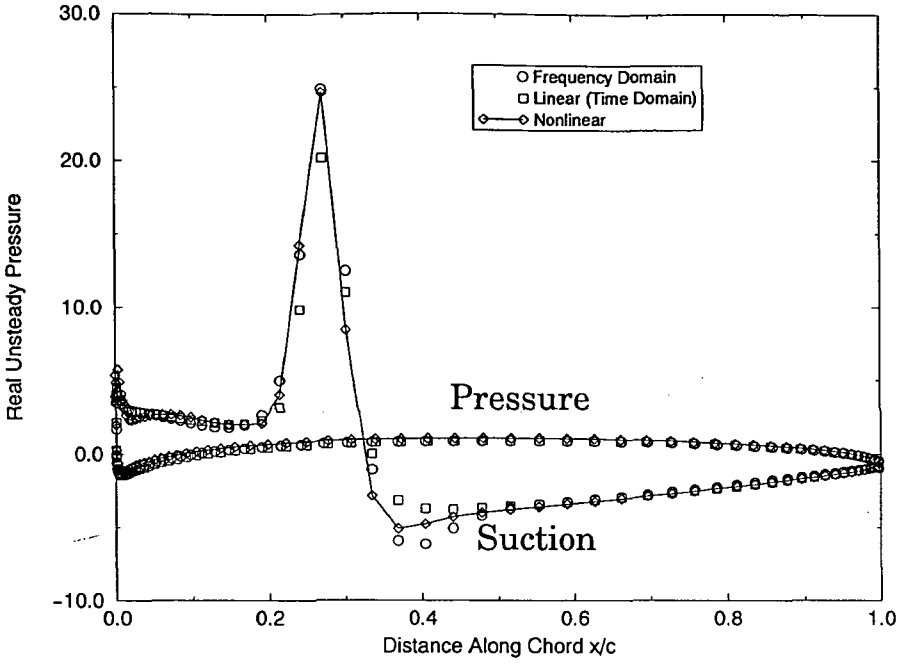

Figure 7.9 Real part of unsteady pressure distribution on transonic 10th std. cfg. due to plunging motion (κ=0.6435, σ=-90°)

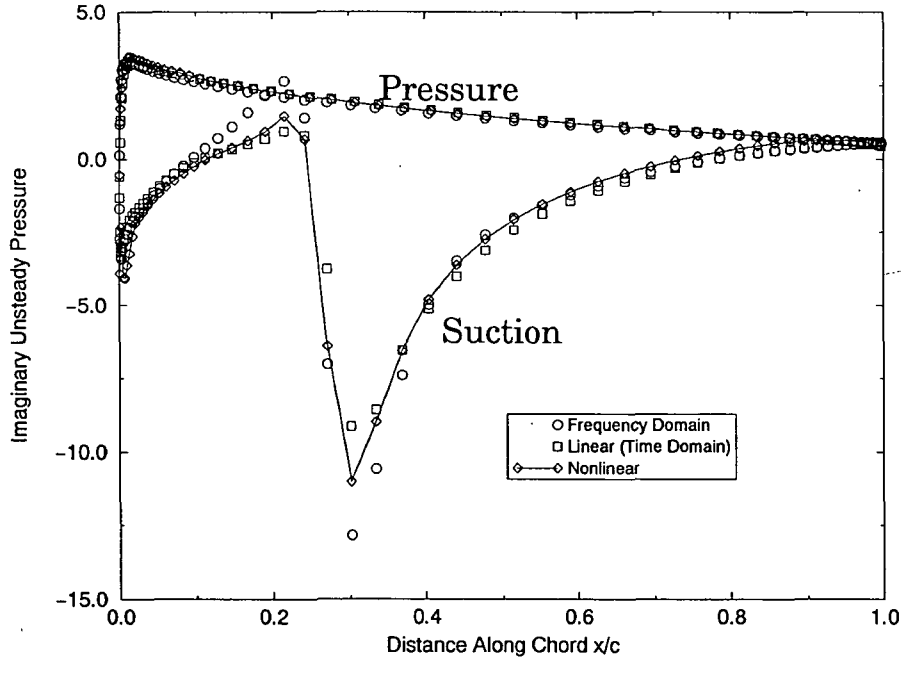

Figure 7.10 Imaginary part of unsteady pressure distribution on transonic 10th std. cfg. due to plunging motion (κ=0.6435, σ=-90°)

CHAPTER VII

CONCLUSIONS

Two linearized Euler solvers (time and frequency domain) based on a high–resolution flux difference split scheme have been presented. The linearized equations are maintained in conservation law form and the same solution procedure is used to solve the nonlinear as well as the linearized equations. Newton subiterations helped improve time–accuracy of both the nonlinear as well as the linearized (time domain) solutions.

The results presented in Chapter 6 prove the feasibility of using the present approaches in solving small amplitude aeroelastic and aeroacoustic problems. Though it has not been tested, no practical difficulties are anticipated in extending this method to three–dimensional problems. The present method performs well over all flow regimes, i.e., subsonic, transonic and supersonic, and various cascade configurations.

As anticipated, the frequency domain based method yields significant performance improvement without any degradation in the quality of the solution, thus making it a valuable design tool.

REFERENCES

[1] Verdon, J.M., "Unsteady Aerodynamic Methods for Turbomachinery Aeroelastic and Aeroacoustic Applications," AIAA Paper 92–0011, January 1992.

[2] Hall, K.C., A Linearized Euler Analysis of Unsteady Flows in Turbomachinery, Sc.D. Thesis, Massachusetts Institute of Technology, May 1987.

[3] Janus, J.M., Advanced 3–D CFD Algorithm for Turbomachinery, Ph.D. Dissertation, Mississippi State University, May 1989.

[4] Belk, D.M., Unsteady Three–Dimensional Euler Equations Solutions on Dynamic Blocked Grids, Ph.D. Dissertation, Mississippi State University, August 1986.

[5] Roe, P.L., "Approximate Riemann Solvers, Parameter Vector, and Difference Schemes," *Journal of Computational Physics*, Vol. 43, pp 357–372, 1981.

[6] Whitfield, D.L., Janus, J.M. and Simpson, L.B., Implicit Finite Vol.ume High Resolution Wave–Split Scheme for Solving the Unsteady Three–Dimensional Euler and Navier–Stokes Equations for Stationary or Dynamic Grids, Engineering and Industrial Research Station Report, MSSU–EIRS–ASE–88–2, Mississippi State University, February 1988.

[7] Osher, S. and Chakravarthy, S.R., "Very High Order Accurate TVD Schemes," ICASE Report 84–44, September 1984.

[8] Chakravarthy, S.R., "A New Class of High Accuracy TVD Schemes for Hyperbolic Consveration Laws," AIAA Paper 85–0363, January 1985.

[9] Sweby, P.K., "High Resolution Schemes Using Flux Limiters for Hyperbolic Conservation Laws," *SIAM Journal of Numerical Analysis*, Vol. 21, No.5, pp 995 – 1011, October 1984.

[10] Sreenivas, K., High Resolution Numerical Simulation of the Linearized Euler Equations in Conservation Law Form, M.S. Thesis, Mississippi State University, July 1993.

[11] Strikwerda, J.C., Finite Difference Schemes and Partial Differential Equations, Wadsworth & Brooks/Cole Mathematics Series, 1989.

[12] Whitfield, D.L. and Janus, J.M., "Three Dimensional Unsteady Euler Equations Solution Using Flux Vector Splitting," AIAA Paper 84–1552, June 1984.

[13] Giles, M., "Non–Reflecting Boundary Conditions for Euler Equation Calculations," AIAA Paper 89–1942–CP, 1989.

[14] Hirsch, C., Numerical Computation of Internal and External Flows, Volume 2: Computational Methods for Inviscid and Viscous Flows, John Wiley & Sons, 1990.

[15] Ramsey, J.K., and Kielb, R.E., "A Computer Program for Calculating Unsteady Aerodynamic Coefficients for Cascades in Supersonic Axial Flow," NASA TM 100204 (Corrected Version), December 1987.

[16] Smith, S.N., "Discrete Frequency Sound Generation in Axial Flow Turbomachines," ARC–R/M–3709, 1971.

[17] Lane, F., "Supersonic Flow Past an Oscillating Cascade with Supersonic Leading–Edge Locus," *Journal of Aeronautical Science*, Vol. 24, No.1, pp 65–66, January 1957.